
Joint Contrastive Learning with Infinite Possibilities

Qi Cai^{1*} Yu Wang^{2*} Yingwei Pan² Ting Yao² Tao Mei²

¹ University of Science and Technology of China, Hefei, China

² JD AI Research, Beijing, China

{cqcai, feather1014, panyw.ustc, tingyao.ustc}@gmail.com, tmei@live.com

Abstract

This paper explores useful modifications of the recent development in contrastive learning via novel probabilistic modeling. We derive a particular form of contrastive loss named Joint Contrastive Learning (JCL). JCL implicitly involves the simultaneous learning of an infinite number of query-key pairs, which poses tighter constraints when searching for invariant features. We derive an upper bound on this formulation that allows analytical solutions in an end-to-end training manner. While JCL is practically effective in numerous computer vision applications, we also theoretically unveil the certain mechanisms that govern the behavior of JCL. We demonstrate that the proposed formulation harbors an innate agency that strongly favors similarity within each instance-specific class, and therefore remains advantageous when searching for discriminative features among distinct instances. We evaluate these proposals on multiple benchmarks, demonstrating considerable improvements over existing algorithms. Code is publicly available at: <https://github.com/caiqi/Joint-Contrastive-Learning>.

1 Introduction

In recent years, supervised learning has seen tremendous progress and made great success in numerous real-world applications. By heavily relying on human annotations, supervised learning allows for convenient end-to-end training of deep neural networks, and has made human-crafted features the least popular in the machine learning community. However, the underlying feature behind the data potentially has a much richer structure than what the sparse labels or rewards describe, while label acquisition is also time-consuming and economically expensive. In contrast, unsupervised learning uses no manually labeled annotations, and aims to characterize the underlying feature distribution completely depending on the data itself. This overcomes several disadvantages that the supervised learning encounters, including overfitting of the specific tasks-led features that cannot be readily transferred to other objectives. Unsupervised learning therefore is an important stepping stone towards more robust and generic representation learning.

Contrastive learning is at the core of several advances in unsupervised learning. The use of contrastive loss dates back to [17]. In brief, the loss function in [17] runs over pairs of samples, returning low values for similar pairs and high values for dissimilar pairs, which encourages invariant features on the low dimensional manifold. The seminal work Noise Contrastive Estimation (NCE) [16] then builds up the foundation of the contemporary contrastive learning, as NCE provides rigorous theoretical justification by posing the contrastive learning problem into the “two-class” problem. InfoNCE [36] roots in the principles of NCE and links the contrastive formulation with mutual information.

However, most existing contrastive learning methods only consider *independently* penalizing the incompatibility of each single positive query-key pair at a time. This does not fully leverage the assumption that all augmentations corresponding to a specific image are statistically dependent on

*Qi Cai and Yu Wang contributed equally to this work. This work was performed at JD AI Research.

each other, and are simultaneously similar to the query. In order to take this advantage of shared similarity across augmentations, we derive a particular form of loss for contrastive learning named Joint Contrastive Learning (JCL). Our launching point is to introduce dependencies among different query-key pairs, so that similarity consistency is encouraged within each instance-specific class. Specifically, our contributions include:

- We consider simultaneously penalizing multiple positive query-key pairs in regard of their “in-pair” dissimilarity. However, carrying multiple query-key pairs in a mini-batch is beyond the practical computational budget. To mitigate this issue, we push the limit and take the number of pairs to infinity. This novel formulation inherently absorbs the impact of large number of positive pairs via a principled probabilistic modeling. We could therefore approach an analytic form of loss that allows for end-to-end training of the deep network.
- We also theoretically unveil plenty of interesting interpretations behind the loss. Empirical evidences are presented that strongly echo these hypotheses.
- Empirical results show that JCL is advantageous when searching for discriminative features and JCL demonstrates considerable boosts over existing algorithms on various benchmarks.

2 Related Work

Self-Supervised Learning. Self-supervised learning is one of the mainstream techniques under the umbrella of unsupervised learning. Self-supervised learning, as its name implies, relies only on the data itself for some form of supervision. For example, one important direction of self-supervised learning focuses on tailoring algorithms for specific pretext tasks. These pretext tasks usually leave out a portion of information from the specific training data and attempt to predict the missing information from the remaining part of the training data itself. Successful representatives along this path include: relative patch prediction [6, 12, 15, 35], rotation prediction [14], inpainting [37], image colorization [11, 24, 27, 28, 46, 47], etc. More recently, numerous self-supervised learning approaches capitalizing on contrastive learning techniques start to emerge. These algorithms demonstrate strong advantages in learning invariant features: [2, 8, 18, 21, 23, 29, 34, 36, 40, 43–45, 48]. The central spirit of these approaches aims to maximize the mutual information of latent representations among different views of the images. Different approaches consider different strategies for constructing distinct views. Take for instance, in CMC [40], RGB images are converted to *Lab* color space and each channel represents a different view of the original image. In the meanwhile, different approaches also design different policies for effectively generating negative pairs, e.g., the techniques used in [8, 18].

Semantic Data Augmentation. Data augmentation has been extensively explored in the context of feature generalization and overfitting reduction for effective deep network training. Recent works [1, 4, 25, 38] show that semantic data augmentation is able to effectively preserve the class identity. Among these work, one observation is that variances in feature space along some certain directions essentially correspond to implementing semantic data augmentations in the ambient space [3, 33]. In [41], interpolation in the embedding space is shown effective in achieving semantic data augmentation. [42] estimates the category-wise distribution of deep features and the augmented features are drawn from the estimated distribution.

Comparison to Existing Works. The proposed JCL benefits from an infinite number of positive pairs constructed for each query. ISDA [42] also involves the implicit usage of infinite number of augmentations shown to be advantageous. However, both our bounding technique and the motivation fundamentally differ from ISDA. JCL aims to develop an efficient self-supervised learning algorithm in the context of contrastive learning, where no category annotation is available. In contrast, ISDA is completely a supervised algorithm. There is also a concurrent work CMC [40] that involves optimization over multiple positive pairs. However, JCL is distinct from CMC in many aspects. In comparison, we derive a rigorous bound on the loss function that enables practical implementation of backpropagation for JCL, where the number of positive pairs is pushed to the infinity. In addition, our motivation closely follows a statistical perspective in a principled way, where positive pairs are statistically dependent. We also justify the legitimacy of our proposed formulation analytically by unveiling certain mechanisms that govern the behavior of JCL. All these ingredients are absent in CMC and significantly distinguish JCL from CMC.

3 Method

In this section, we explore and develop the theoretical derivation of our algorithm JCL. We also characterize how the loss function behaves in a way that favors feature generalization. The empirical evidence corroborates the relevant hypotheses stemming from our theoretical analyses.

3.1 Preliminaries

Contrastive learning and its recent variants aim to learn an embedding by separating samples from different distributions via a contrastive loss \mathcal{L} . Assuming we have *query* vectors $\mathbf{q} \in \mathcal{R}^d$, and *key* vectors $\mathbf{k} \in \mathcal{R}^d$, where d is the dimension of the embedding space. The objective \mathcal{L} is a function that aims to reflect incompatibility of each (\mathbf{q}, \mathbf{k}) pair. In this regard, the key vector set \mathcal{K} is constructed as a composition of positive and negative keys, i.e., $\mathcal{K} = \mathcal{K}^+ \cup \mathcal{K}^-$, where the set \mathcal{K}^+ comprises of positive keys \mathbf{k}_i^+ coming from the same distribution as the specific \mathbf{q}_i , ($i = 1, 2, \dots, N$), whereas \mathcal{K}^- represents the set of negative samples \mathbf{k}_i^- from an alternative noise distribution. A desirable \mathcal{L} usually returns low values when a query \mathbf{q}_i is similar to its positive key \mathbf{k}_i^+ while it remains distinct to negative keys \mathbf{k}_i^- in the meanwhile.

The theoretical foundation of Noise Contrastive Learning (NCE), where negative samples are viewed as noises with regard to each query, is firstly established in [16]. In [16], the learning problem becomes a “two-class” task, where the goal is to distinguish true samples out of the empirical distribution from the noise distribution. Inspired by [16], a prevailing form of \mathcal{L} is presented in InfoNCE [36] based on a softmax formulation:

$$\mathcal{L} = -\frac{1}{N} \sum_i \log \frac{\exp(\mathbf{q}_i^T \mathbf{k}_i^+ / \tau)}{\exp(\mathbf{q}_i^T \mathbf{k}_i^+ / \tau) + \sum_{j=1}^K \exp(\mathbf{q}_i^T \mathbf{k}_{i,j}^- / \tau)}, \quad (1)$$

where \mathbf{q}_i is the i^{th} query in the dataset, \mathbf{k}_i^+ is the positive key corresponding to \mathbf{q}_i , $\mathbf{k}_{i,j}^-$ is the j^{th} negative key of \mathbf{q}_i . The motivation behind Eq.(1) is straightforward: training a network with parameters that could correctly distinguish positive samples from the K negative samples, i.e., from the *noise* set $\mathcal{K}^- = \{\mathbf{k}_{i,1}^-, \mathbf{k}_{i,2}^-, \dots, \mathbf{k}_{i,K}^-\}$. τ is the temperature hyperparameter following [8, 18].

Orthogonal to the design of the formulation \mathcal{L} itself though, one of the remaining challenges is to construct \mathcal{K}^+ and \mathcal{K}^- efficiently in an unsupervised way. Since no annotation is available in an unsupervised learning setting, one common practice is to generate independent augmented views from each single training sample, e.g., an image \mathbf{x}_i , and consider each random pairing of these augmentations as a valid positive $(\mathbf{q}_i, \mathbf{k}_i^+)$ pair in Eq.(1). In the meanwhile, augmented views of other samples $\mathbf{x}_j, j \neq i$ are seen as the negative keys \mathbf{k}_i^- that form the noise distribution against the query \mathbf{q}_i . Under this construction, each image essentially defines an individual class, and each image’s distinct augmentations form the corresponding instance-specific distribution. Take for instance, SimCLR [8] uses distinct images in current mini-batch as negative keys. MoCo [18] proposes the use of a queue \mathcal{Q} in order to track negative samples from neighboring mini-batches. During training, each mini-batch is subsequently enqueued into \mathcal{Q} while the oldest batch of samples in \mathcal{Q} are dequeued. In this way, all the currently queuing samples serve as negative keys and effectively decouples the correlation between mini-batch size and the number of negative keys. Correspondingly, MoCo exclusively enjoys an extremely large number of negative samples that best approaches the theoretical bound justified in [16]. This queuing trick also allows for feasible training on a typical 8-GPU machine and achieves state-of-the-art learning performances. We therefore adopt the MoCo’s approach of constructing negative keys in this paper, owing to its effectiveness and ease of implementation.

3.2 Joint Contrastive Learning

Conventional formulation in Eq.(1) independently penalizes the incompatibility within each $(\mathbf{q}_i, \mathbf{k}_i^+)$ pair at a time. We instead derive a particular form of the contrastive loss where multiple positive keys are simultaneously involved with regard to \mathbf{q}_i . The goal of this modification is to force various positive keys to build up stronger dependencies via the bond with the same \mathbf{q}_i . The new objective poses a tighter constraint on instance-specific features, and tends to encourage the consistent representations within each instance-specific class during the search for invariant features.

In our framework, every query \mathbf{q}_i now needs to return a low loss value when simultaneously paired with multiple positive keys $\mathbf{k}_{i,m}^+$ of its own, where subscript m indicates the m^{th} positive key paired

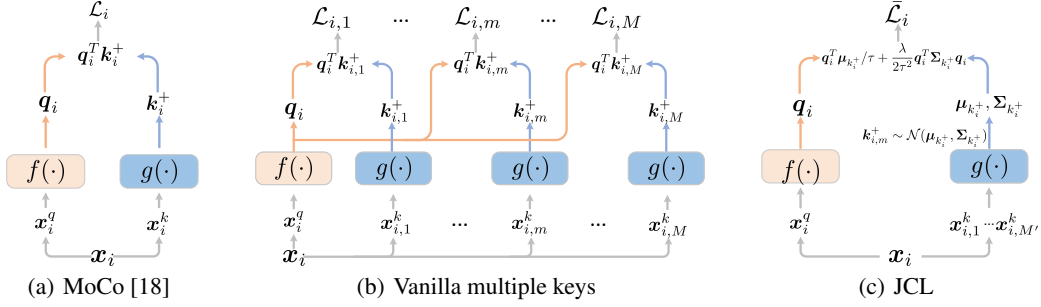


Figure 1: Conceptual comparisons of three contrastive loss mechanisms. (a) In MoCo, a single positive key k_i^+ is paired with a query q_i . (b) A vanilla extension which generates multiple keys and averages losses of all $(q_i, k_{i,m}^+)$ pairs. (c) JCL implicitly pushes the number of $k_{i,m}^+$ to infinity and minimizes the upper bound of loss expectation.

with q_i . Specifically, we define the loss of each pair $(q_i, k_{i,m}^+)$ as:

$$\mathcal{L}_{i,m} = -\log \frac{\exp(\mathbf{q}_i^T \mathbf{k}_{i,m}^+ / \tau)}{\exp(\mathbf{q}_i^T \mathbf{k}_{i,m}^+ / \tau) + \sum_{j=1}^K \exp(\mathbf{q}_i^T \mathbf{k}_{i,j}^- / \tau)}. \quad (2)$$

Our objective is to penalize the averaged sum of $\mathcal{L}_{i,m}$:

$$\mathcal{L}_i^M = \frac{1}{M} \sum_{m=1}^M \mathcal{L}_{i,m} \quad (3)$$

with regard to each specific query q_i . This procedure is illustrated in Fig.(1(b)): a specific training sample x_i is firstly augmented in the ambient space into respectively: the query image x_i^q , and the positive key images $x_i^{k,1}, x_i^{k,2}, \dots, x_i^{k,m}$. Each of the query image x_i^q is subsequently mapped into embedding q_i via the query encoder $f(\cdot)$, while each positive key image $x_i^{k,m}$ is mapped into embedding $k_{i,m}^+$ via key encoder $g(\cdot)$. Both functions f and g are implemented using deep neural networks, of which the network parameters are learned during training. For comparison, Fig.(1(a)) shows the schemes of MoCo where only a single positive key is involved.

A vanilla implementation of \mathcal{L}_i^M would have required the instance x_i to be firstly augmented $M + 1$ times (M for positive keys and 1 extra for the query itself), and then to backpropagate the loss Eq.(3) via all the branches in Fig.(1(b)). Unfortunately, this is not computational applicable, as carrying all $(M + 1) \times N$ pairs in a mini-batch would quickly drain the GPU memory when M is even moderately small. In order to circumvent this issue, we take an infinity limit on the number M , where the effect of M is hopefully absorbed in a probabilistic way. Capitalizing on this application of infinity limit, the statistics of the data become sufficient to reach the same goal of multiple pairing. Mathematically, as M goes to infinity, \mathcal{L}_i^M becomes the estimate of:

$$\mathcal{L}_i^\infty = \lim_{M \rightarrow \infty} \frac{1}{M} \sum_{m=1}^M \mathcal{L}_{i,m} = -\mathbb{E}_{\mathbf{k}_i^+ \sim p(\mathbf{k}_i^+)} \log \frac{\exp(\mathbf{q}_i^T \mathbf{k}_i^+ / \tau)}{\exp(\mathbf{q}_i^T \mathbf{k}_i^+ / \tau) + \sum_{j=1}^K \exp(\mathbf{q}_i^T \mathbf{k}_{i,j}^- / \tau)}. \quad (4)$$

The analytic form of Eq.(4) itself is intractable, but Eq.(4) has a rigorous closed form of upper bound, which can be derived as:

$$-\mathbb{E}_{\mathbf{k}_i^+} \log \frac{\exp(\mathbf{q}_i^T \mathbf{k}_i^+ / \tau)}{\exp(\mathbf{q}_i^T \mathbf{k}_i^+ / \tau) + \sum_{j=1}^K \exp(\mathbf{q}_i^T \mathbf{k}_{i,j}^- / \tau)} \quad (5)$$

$$= \mathbb{E}_{\mathbf{k}_i^+} \left[\log \left[\exp(\mathbf{q}_i^T \mathbf{k}_i^+ / \tau) + \sum_{j=1}^K \exp(\mathbf{q}_i^T \mathbf{k}_{i,j}^- / \tau) \right] \right] - \mathbb{E}_{\mathbf{k}_i^+} \left[(\mathbf{q}_i^T \mathbf{k}_i^+ / \tau) \right] \quad (6)$$

$$\leq \log \left[\mathbb{E}_{\mathbf{k}_i^+} \left[\exp(\mathbf{q}_i^T \mathbf{k}_i^+ / \tau) + \sum_{j=1}^K \exp(\mathbf{q}_i^T \mathbf{k}_{i,j}^- / \tau) \right] \right] - \mathbf{q}_i^T \mathbb{E}_{\mathbf{k}_i^+} \left[\mathbf{k}_i^+ / \tau \right], \quad (7)$$

where Eq.(7) upperbounds \mathcal{L}_i^∞ . The inequality Eq.(7) emerges from the application of Jensen inequality on concave functions, i.e., $\mathbb{E}_x \log(X) \leq \log \mathbb{E}_x[X]$. This application of Jensen inequality does not interfere with the effectiveness of our algorithm and rather buys us desired optimization advantages. We analyze this part in detail in section 3.3.

Algorithm 1 Joint Contrastive Learning

```
1: Input: batch size  $N$ , positive key number  $M'$ , queue  $\mathcal{Q}$ , query encoder  $f(\cdot)$ , key encoder  $g(\cdot)$ ,
2: for sampled mini-batch  $\{\mathbf{x}_i\}_{i=1}^N$  do
3:   for each sample  $\mathbf{x}_i$  do
4:     randomly augment  $\mathbf{x}_i$  for  $M' + 1$  times:  $\{\mathbf{x}_i^q, \mathbf{x}_{i,1}^k, \mathbf{x}_{i,2}^k, \dots, \mathbf{x}_{i,M'}^k\}$ 
5:     compute query representation:  $\mathbf{q}_i = f(\mathbf{x}_i^q)$ 
6:     compute key representations:  $\mathbf{k}_{i,m}^+ = g(\mathbf{x}_{i,m}^k), \dots, \mathbf{k}_{i,M'}^+ = g(\mathbf{x}_{i,M'}^k)$ 
7:     compute average values of keys:  $\boldsymbol{\mu}_{k_i^+} = \frac{1}{M'} \sum_{m=1}^{M'} \mathbf{k}_{i,m}^+$ 
8:     compute zero centered keys:  $\tilde{\mathbf{k}}_{i,m}^+ = \mathbf{k}_{i,m}^+ - \boldsymbol{\mu}_{k_i^+}, m = 1, 2, \dots, M'$ 
9:     compute covariance matrix:  $\boldsymbol{\Sigma}_{k_i^+} = \frac{1}{M'} [\tilde{\mathbf{k}}_{i,1}^+, \dots, \tilde{\mathbf{k}}_{i,M'}^+]^T [\tilde{\mathbf{k}}_{i,1}^+, \dots, \tilde{\mathbf{k}}_{i,M'}^+]$ 
10:    compute loss  $\bar{\mathcal{L}}_i$  based on Eq.(8)
11:  end for
12:  compute loss  $\bar{\mathcal{L}}$  in Eq.(9) and update  $f(\cdot), g(\cdot)$  based on  $\bar{\mathcal{L}}$ 
13:  enqueue  $\{\boldsymbol{\mu}_{k_i^+}\}_{i=1}^N$  and dequeue oldest keys in  $\mathcal{Q}$ 
14: end for
15: return  $f(\cdot)$ 
```

To facilitate our formulation, we need some further assumptions on the generative process of \mathbf{k}_i^+ in the feature space \mathcal{R}^d . Specifically, we assume the variable \mathbf{k}_i^+ follows a Gaussian distribution $\mathbf{k}_i^+ \sim \mathcal{N}(\boldsymbol{\mu}_{k_i^+}, \boldsymbol{\Sigma}_{k_i^+})$, where $\boldsymbol{\mu}_{k_i^+}$ and $\boldsymbol{\Sigma}_{k_i^+}$ are respectively the mean and the covariance matrix of the positive keys for \mathbf{q}_i . This Gaussian assumption explicitly poses statistical dependencies among all the \mathbf{k}_i^+ s, and makes the learning process appealing to consistency between positive keys. We argue that this assumption is legitimate as positive keys more or less share similarities in the embedding space around some mean value as they all mirror the nature of the query to some extent. Also there are certainly some reasonable variances expected in each feature dimension that reflects the semantic difference in the ambient space [3, 33]. In brief, we randomly augment each \mathbf{x}_i in the ambient space (e.g., pixel values for images) for M' times (M' is relatively small) and compute the covariance matrix $\boldsymbol{\Sigma}_{k_i^+}$ on the fly. Since the statistics are more informative in the later of the training/less informative in the beginning of the training, we scale the influence of $\boldsymbol{\Sigma}_{k_i^+}$ by multiplying it with a scalar λ . This tuning of λ hopefully stabilizes the training. Under this Gaussian assumption, Eq.(7) eventually reduces to (see supplementary material for more detailed derivations):

$$\bar{\mathcal{L}}_i = \log \left[\exp(\mathbf{q}_i^T \boldsymbol{\mu}_{k_i^+} / \tau + \frac{\lambda}{2\tau^2} \mathbf{q}_i^T \boldsymbol{\Sigma}_{k_i^+} \mathbf{q}_i) + \sum_{j=1}^K \exp(\mathbf{q}_i^T \mathbf{k}_{i,j}^- / \tau) \right] - \mathbf{q}_i^T \boldsymbol{\mu}_{k_i^+} / \tau. \quad (8)$$

The overall loss function with regard to each mini-batch (N is the batch size) therefore boils down to the closed form whose gradients can be analytically solved for:

$$\bar{\mathcal{L}} = \frac{1}{N} \sum_{i=1}^N \bar{\mathcal{L}}_i. \quad (9)$$

Algorithm 1 summarizes the algorithmic flow of the JCL procedure. It is important to note that, the computational cost when using M' number of positive keys to compute the sufficient statistics, is fundamentally different from backpropagating losses of $(M' + 1) \times N$ pairs (which vanilla formulation shown as in Fig.(1(b)) would have done) from the perspective of memory schedules and cost (see more detailed comparisons in supplementary material). For comparison, we illustrate the actual JCL computation in Fig.(1(c)).

3.3 Analysis

We emphasize that the introduction of Jensen inequality in Eq.(7) actually unveils a number of interesting interpretations behind the loss. Firstly, by virtue of the Jensen inequality, the equality in Eq.(7) holds if and only if the variable \mathbf{k}_i^+ is a *constant*, i.e., when all the positive keys $\mathbf{k}_{i,m}^+$ of \mathbf{q}_i produce identical embedding $\mathbf{k}_{i,m}^+$. This translates into a desirable incentive: in order to close the gap between Eq.(6) and Eq.(7) so that the loss is decreased, the training process mostly favors invariant representation across different positive keys, i.e., very similar $\mathbf{k}_{i,m}^+$ s given different augmentations.

Also, the loss reserves a strong incentive to push queries away from noisy negative samples, as the loss is monotonously decreasing as $\sum_{j=1}^K \exp(\mathbf{q}_i^T \mathbf{k}_{i,j}^-)$ reduces. Most importantly, after some basic manipulation, it is easy to show that \mathcal{L}_i is also monotonously decreasing into the direction where $\mathbf{q}_i^T \boldsymbol{\mu}_{k_i^+}$ increases, i.e., when \mathbf{q}_i and $\boldsymbol{\mu}_{k_i^+}$ closely resembles each other.

We argue that conventional contrastive loss does not enjoy similar merits. Although as the training proceeds with more epochs, the \mathbf{q}_i might be randomly paired with a numerous distinct \mathbf{k}_i^+ , the loss Eq.(1) simply goes downhill as long as each \mathbf{q}_i aligns independently with each positive key \mathbf{k}_i^+ at a time. This likely confuses the learning procedure and sabotage the effectiveness in finding a unified direction for all positive keys.

4 Experiments

In this section, we empirically evaluate and analyze the hypotheses that directly emanated from the design of JCL. One important purpose of unsupervised learning is to pre-train features that can be transferred to downstream tasks. Correspondingly, we demonstrate that in numerous downstream tasks related to classification, detection and segmentation, JCL exhibits strong advantages and surpasses the state-of-the-art approaches. Specifically, we perform the pre-training on ImageNet1K [10] dataset that contains 1.2M images evenly distributed across 1,000 classes. Following the protocols in [8, 18], we verify the effectiveness of JCL pre-trained features via the following evaluations: **1)** Linear classification accuracy on ImageNet1K. **2)** Generalization capability of features when transferred to alternative downstream tasks, including object detection [5, 39], instance segmentation [19] and keypoint detection [19] on the MS COCO [31] dataset. **3)** Ablation studies that reveal the effectiveness of each component in our losses. **4)** Statistical analysis on features that validates our hypothesis and proposals in the previous sections. For more detailed experimental settings, please refer to the supplementary material.

4.1 Pre-Training Setups

We adopt ResNet-50 [20] as the backbone network for training JCL on the ImageNet1K dataset. For the hyper-parameters, we use positive key number $M' = 5$, softmax temperature $\tau = 0.2$ and $\lambda = 4.0$ in Eq.(8) (see definitions in section 3.2). We also investigate the impact of these hyper-parameters tuning in section 4.4. Other network and parameter settings strictly follow the implementations in MoCo v2 [9] for fair apple to apple comparisons. We attach a two-layer MLP (Multiple Layer Perceptrons) on top of the global pooling layer of ResNet-50 for generating the final embeddings. The dimension of this embedding is $d = 128$ across all experiments. The batch size is set to $N = 512$ that enables applicable implementations on an 8-GPU machine. We train JCL for 200 epochs with an initial learning rate of $lr = 0.06$ and lr is gradually annealed following a cosine decay schedule [32].

4.2 Linear Classification on ImageNet1K

Setup. In this section, we follow [8, 18] and train a linear classifier on frozen features extracted from ImageNet1K. Specifically, we initialize the layers before the global poolings of ResNet-50 with the parameter values obtained from our JCL pre-trained model, and then append a fully connected layer on top of the resultant ResNet-50 backbone. During training, the parameters of the backbone network are frozen, while only the last fully connected layer is updated via backpropagation. The batch size is set as $N = 256$ and the learning rate $lr = 30$ at this stage. In this way, we essentially train a linear classifier on frozen features. The classifier is trained for 100 epochs, while the learning rate lr is decayed by 0.1 at the 60th and the 80th epoch respectively.

Results. Table 1 reports the top-1 accuracy and top-5 accuracy in comparison with the state-of-the-art methods. Existing works differ considerably in model size and the training epochs, which could significantly influence the performance (up to 8% in [18]). We therefore only consider comparisons to the published models of similar model size and training epochs. As Table 1 shows, JCL performs the best among all the presented approaches. Particularly, JCL outperforms all *non-contrastive learning based* counterparts by a large margin, which demonstrates evident advantages brought by the idea of contrastive learning itself. The introduction of positive and negative pairs more effectively recovers each instance-specific distributions. Most notably, JCL remains competitive and surpasses all its *contrastive learning based* rivals, e.g., MoCo and MoCo v2. This superiority of JCL over its MoCo baselines clearly verifies the advantage of our proposal Eq.(8) via the joint learning process across numerous positive pairs.

Table 1: Accuracy of linear classification model on ImageNet1K. [†] represents results from [26], which reports better performances than the original papers. [‡] means accuracies of models trained 200 epochs for fair comparisons. [§] denotes results of our re-implemented linear classifier based on pre-trained model from <https://github.com/facebookresearch/moco> for extracting features.

Method	architecture	params (M)	accuracy@top1	accuracy@top5
RelativePosition [12]	ResNet-50(2x)	94	51.4 [†]	74.0 [†]
Jigsaw [35]	ResNet-50(2x)	94	44.6 [†]	68.0 [†]
Rotation [14]	RevNet(4x)	86	55.4 [†]	77.9 [†]
Colorization [46]	ResNet-101	28	39.6	/
DeepCluster [7]	VGG	15	48.4	/
BigBiGAN [13]	RevNet(4x)	86	61.3	81.9
<i>methods based on contrastive learning follow:</i>				
InstDisc [43]	ResNet-50	24	54.0	/
LocalAgg [48]	ResNet-50	24	60.2	/
CPC v1 [36]	ResNet-101	28	48.7	73.6
CPC v2 [21]	ResNet-50	24	63.8	85.3
CMC [40]	ResNet-50	47	64.0	85.5
SimCLR [8]	ResNet-50	24	66.6 [‡]	/
MoCo [18]	ResNet-50	24	60.6 [‡] (60.6 [§])	83.1 [§]
MoCo v2 [9]	ResNet-50	24	67.5 [‡] (67.6 [§])	88.0 [§]
JCL	ResNet-50	24	68.7	89.0

Table 2: Performance comparisons on downstream tasks: object detection [39](left), instance segmentation [19](middle) and keypoint detection [19](right). All models are trained with $1\times$ schedule.

model	<i>Faster R-CNN + R-50</i>			<i>Mask R-CNN + R-50</i>			<i>Keypoint R-CNN + R-50</i>		
	AP ^{bb}	AP ₅₀ ^{bb}	AP ₇₅ ^{bb}	AP ^{mk}	AP ₅₀ ^{mk}	AP ₇₅ ^{mk}	AP ^{kp}	AP ₅₀ ^{kp}	AP ₇₅ ^{kp}
random	30.1	48.6	31.9	28.5	46.8	30.4	63.5	85.3	69.3
supervised	38.2	59.1	41.5	35.4	56.5	38.1	65.4	87.0	71.0
MoCo [18]	37.1	57.4	40.2	35.1	55.9	37.7	65.6	87.1	71.3
MoCo v2 [9]	37.6	57.9	40.8	35.3	55.9	37.9	66.0	87.2	71.4
JCL	38.1	58.3	41.3	35.6	56.2	38.3	66.2	87.2	72.3

4.3 More Downstream Tasks

In this section, we evaluate JCL on a variety of more downstream tasks, i.e., object detection, instance segmentation and keypoint detection. The comparisons presented here cover a wide range of computer vision tasks from box-level to pixel-level, as we aim to challenge JCL from all dimensions.

Setup. For object detection, we adopt Faster R-CNN [39] with FPN [30] as the base detector. Following [18], we leave the BN trained and add batch normalization on FPN layers. The size of the shorter side of each image is sampled from the range [640, 800] during training and is fixed as 800 at inference time, while the longer side of the image always keeps proportional to the shorter side. The training is performed on a 4-GPU machine and each GPU carries 4 images at a time. This implementation is equivalent to batch size $N = 16$. We train all models for 90k iterations, which is commonly referred to as the $1\times$ schedule in [18]. For the instance segmentation and keypoint detection tasks, we adopt the same settings as Faster R-CNN [39] has used. We report the standard COCO metrics including AP (averaged over [0.5:0.95:0.05] $IoUs$), AP₅₀($IoU=0.5$) and AP₇₅($IoU=0.75$).

Results. Table 2 shows the results for three downstream tasks on MS COCO. From observation, both supervised pre-trained models (**supervised**) and unsupervised pre-trained backbones (**MoCo**, **MoCo v2**, **JCL**) exhibit a significant performance boost against the randomly initialized models (**random**). Our proposed JCL demonstrates clear superiority over the best competitor MoCo v2. When taking a closer inspection, JCL becomes particularly advantageous when a higher IoU threshold criterion is used for object detection. This might attribute to a more precise sampling of positive pairs, under which JCL is able to promote a more accurate positive pairing and joint training. Notably, JCL even successfully surpasses its supervised counterparts in terms of AP^{mk}, whereas MoCo v2 remains inferior to the supervised pre-training approaches.

In brief, JCL has presented robust performance gain over existing methods across numerous important benchmark tasks. In the following section, we further investigate the impact of hyperparameters and provide validations that closely corroborate our hypothesis pertaining to the design of JCL.

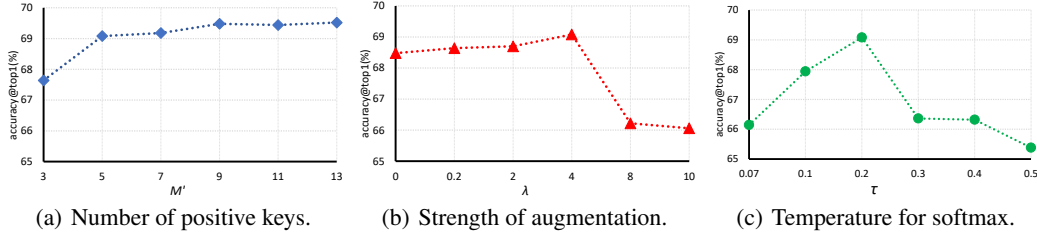


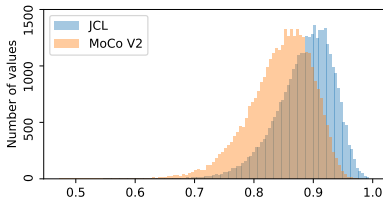
Figure 2: Performance comparisons with different hyperparameters.

4.4 Ablation Studies

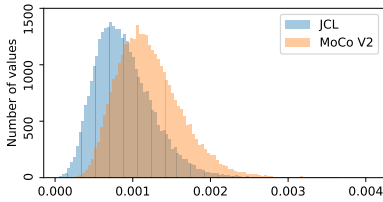
In this section, we perform extensive ablation experiments to inspect the role of each component present in the JCL loss. Specifically, we test JCL on linear classification in ImageNet100 deployed on ResNet-18. For detailed experiment settings, please see supplementary material.

1) M' : We vary the number of positive keys used for the estimate of $\mu_{k_i^+}$ and $\Sigma_{k_i^+}$. By definition, larger M' necessarily corresponds to a better approximation of the required statistics, although at the expense of computational complexity. From Fig.(2(a)), we observe that JCL performs reasonably well when M' is in the range of [5,11], which allows for applicable GPU implementation. **2) λ :** λ essentially controls the strength of augmentation diversity in the feature space. Larger λ tends to inject more diverse features into the effect of positive pairing, but risks confusions with other instance distributions. Here, we vary λ in the range of [0.0, 10.0]. Notice that in the case when λ is marginally small, the effect of scaled covariance matrix is diminished and therefore fails to introduce the feature variance among distinct positive samples of the same query. However, an extremely large λ overstates the effect of diversity that rather confuses the positive sample distribution with the negative samples. As the introduced variance $\Sigma_{k_i^+}$ starts to *dominate* the positive mean $\mu_{k_i^+}$ value, i.e., when the λ is large enough to distort the magnitude scale of positive keys, the impact of negative keys in Eq.(8) is diluted. Consequently, the distribution of the $k_{i,m}^+$ and $k_{i,j}^-$ would also significantly be distorted. When λ grows to infinity, the effect of negative keys completely vanishes owing to the overwhelming λ and the associated positive keys, and JCL has no motivation to distinguish between positive and negative keys. From Fig.(2(b)), we can see that the performance is relatively stable in a wide range of [0.2,4.0]. **3) τ :** The temperature τ [22] affects the flatness of softmax function and the confidence of each positive pair. From Fig.(2(c)), the optimal τ turns out to be around 0.2. As τ increases beyond 0.2, the classification accuracy starts to drop, owing to an increasing uncertainty and reduced confidence of the positive pairs. When the value τ becomes too small, the algorithm tends to overweight the influence of each positive pair and degrade the pre-training.

4.5 Feature Distribution



(a) Similarity distribution



(b) Variance distribution

Figure 3: Distribution of positive pair similarities and feature variances.

cosine similarities. It is clear that JCL achieves much more samples with higher similarity scores than that of the MoCo v2. This implies that JCL indeed tends to favor a more consistent feature invariance

within each instance-specific distribution. We also extract the diagonal entries from $\Sigma_{k_i^+}$ and display the histogram in Fig.(3(b)). Accordingly, the variance of the obtained features belonging to the same image is much smaller, as shown in Fig.(3(b)). This also aligns with our hypothesis that JCL favors consistent representations across different positive keys.

5 Conclusions

We propose a particular form of contrastive loss named joint contrastive learning (JCL). JCL implicitly involves the joint learning of an infinite number of query-key pairs for each instance. By applying rigorous bounding techniques on the proposed formulation, we transfer the originally intractable loss function into practical implementations. We empirically demonstrate the correctness of our bounding technique along with the superiority of JCL on various benchmarks. These empirical evidences also qualitatively support our theoretical hypothesis behind the central mechanism of JCL. Most notably, although JCL is an unsupervised algorithm, the JCL pre-trained networks even outperform its supervised counterparts in many scenarios.

6 Broader Impact

Supervised learning has seen tremendous success in the AI community. By heavily relying on human annotations, supervised learning allows for convenient end-to-end training of deep neural networks. However, label acquisition is usually time-consuming and economically expensive. Particularly, when the algorithm needs to pre-train on massive datasets such as ImageNet, obtaining the labels for millions of data becomes an extremely tedious and expensive prerequisite that hinders one from trying out interesting ideas. This significantly limits and discourages the motivations for relatively small research communities without adequate financial supports. Another concern is the accuracy of the annotations, as labeling millions of data might very likely induce noisy and wrong labels owing to mistakes. What we have proposed in this paper is an unsupervised algorithm called JCL that solely depends on data itself without human annotations. JCL offers an alternative way to more efficiently exploit the pre-training dataset in an unsupervised way. One can even build up his/her own pre-training dataset by crawling data randomly from internet without any labeling efforts. However, one potential risk lies in the fact that if the usage of unsupervised visual representation learning aims at visual understanding systems (e.g., image classification and object detection), these systems may now be easily approached by those with lower levels of domain knowledge or machine learning expertise. This could expose the visual understanding model to some inappropriate usage and occasions without proper regulation or expertise.

References

- [1] Antreas Antoniou, Amos Storkey, and Harrison Edwards. Data augmentation generative adversarial networks. In *arXiv preprint arXiv:1711.04340*, 2017.
- [2] Philip Bachman, R Devon Hjelm, and William Buchwalter. Learning representations by maximizing mutual information across views. In *NeurIPS*, 2019.
- [3] Yoshua Bengio, Grégoire Mesnil, Yann Dauphin, and Salah Rifai. Better mixing via deep representations. In *ICML*, 2013.
- [4] Konstantinos Bousmalis, Nathan Silberman, David Dohan, Dumitru Erhan, and Dilip Krishnan. Unsupervised pixel-level domain adaptation with generative adversarial networks. In *CVPR*, 2017.
- [5] Qi Cai, Yingwei Pan, Yu Wang, Jingen Liu, Ting Yao, and Tao Mei. Learning a unified sample weighting network for object detection. In *CVPR*, 2020.
- [6] Fabio M Carlucci, Antonio D’Innocente, Silvia Bucci, Barbara Caputo, and Tatiana Tommasi. Domain generalization by solving jigsaw puzzles. In *CVPR*, 2019.
- [7] Mathilde Caron, Piotr Bojanowski, Armand Joulin, and Matthijs Douze. Deep clustering for unsupervised learning of visual features. In *Proceedings of the ECCV (ECCV)*, 2018.

- [8] Ting Chen, Simon Kornblith, Mohammad Norouzi, and Geoffrey Hinton. A simple framework for contrastive learning of visual representations. In *arXiv preprint arXiv:2002.05709*, 2020.
- [9] Xinlei Chen, Haoqi Fan, Ross Girshick, and Kaiming He. Improved baselines with momentum contrastive learning. In *arXiv preprint arXiv:2003.04297*, 2020.
- [10] Jia Deng, Wei Dong, Richard Socher, Li-Jia Li, Kai Li, and Li Fei-Fei. Imagenet: A large-scale hierarchical image database. In *CVPR*, 2009.
- [11] Aditya Deshpande, Jason Rock, and David Forsyth. Learning large-scale automatic image colorization. In *ICCV*, 2015.
- [12] Carl Doersch, Abhinav Gupta, and Alexei A Efros. Unsupervised visual representation learning by context prediction. In *ICCV*, 2015.
- [13] Jeff Donahue and Karen Simonyan. Large scale adversarial representation learning. In *NeurIPS*, 2019.
- [14] Spyros Gidaris, Praveer Singh, and Nikos Komodakis. Unsupervised representation learning by predicting image rotations. In *ICLR*, 2018.
- [15] Priya Goyal, Dhruv Mahajan, Abhinav Gupta, and Ishan Misra. Scaling and benchmarking self-supervised visual representation learning. In *ICCV*, 2019.
- [16] Michael Gutmann and Aapo Hyvärinen. Noise-contrastive estimation: A new estimation principle for unnormalized statistical models. In *AISTATS*, 2010.
- [17] Raia Hadsell, Sumit Chopra, and Yann LeCun. Dimensionality reduction by learning an invariant mapping. In *CVPR*, 2006.
- [18] Kaiming He, Haoqi Fan, Yuxin Wu, Saining Xie, and Ross Girshick. Momentum contrast for unsupervised visual representation learning. In *CVPR*, 2020.
- [19] Kaiming He, Georgia Gkioxari, Piotr Dollár, and Ross Girshick. Mask r-cnn. In *ICCV*, 2017.
- [20] Kaiming He, Xiangyu Zhang, Shaoqing Ren, and Jian Sun. Deep residual learning for image recognition. In *CVPR*, 2016.
- [21] Olivier J Hénaff, Aravind Srinivas, Jeffrey De Fauw, Ali Razavi, Carl Doersch, SM Eslami, and Aaron van den Oord. Data-efficient image recognition with contrastive predictive coding. In *CVPR*, 2019.
- [22] Geoffrey Hinton, Oriol Vinyals, and Jeff Dean. Distilling the knowledge in a neural network. *arXiv preprint arXiv:1503.02531*, 2015.
- [23] R Devon Hjelm, Alex Fedorov, Samuel Lavoie-Marchildon, Karan Grewal, Phil Bachman, Adam Trischler, and Yoshua Bengio. Learning deep representations by mutual information estimation and maximization. In *ICLR*, 2019.
- [24] Satoshi Iizuka, Edgar Simo-Serra, and Hiroshi Ishikawa. Let there be color! joint end-to-end learning of global and local image priors for automatic image colorization with simultaneous classification. In *ToG*, 2016.
- [25] Max Jaderberg, Karen Simonyan, Andrea Vedaldi, and Andrew Zisserman. Reading text in the wild with convolutional neural networks. In *IJCV*, 2016.
- [26] Alexander Kolesnikov, Xiaohua Zhai, and Lucas Beyer. Revisiting self-supervised visual representation learning. In *CVPR*, 2019.
- [27] Gustav Larsson, Michael Maire, and Gregory Shakhnarovich. Learning representations for automatic colorization. In *ECCV*, 2016.
- [28] Gustav Larsson, Michael Maire, and Gregory Shakhnarovich. Colorization as a proxy task for visual understanding. In *CVPR*, 2017.

- [29] Michael Laskin, Aravind Srinivas, and Pieter Abbeel. Curl: Contrastive unsupervised representations for reinforcement learning. In *The proceedings of the International Conference on Machine Learning (ICML)*, 2020.
- [30] Tsung-Yi Lin, Piotr Dollár, Ross Girshick, Kaiming He, Bharath Hariharan, and Serge Belongie. Feature pyramid networks for object detection. In *CVPR*, 2017.
- [31] Tsung-Yi Lin, Michael Maire, Serge Belongie, James Hays, Pietro Perona, Deva Ramanan, Piotr Dollár, and C Lawrence Zitnick. Microsoft coco: Common objects in context. In *ECCV*, 2014.
- [32] Ilya Loshchilov and Frank Hutter. Sgdr: Stochastic gradient descent with warm restarts. In *ICLR*, 2017.
- [33] Laurens Maaten, Minmin Chen, Stephen Tyree, and Kilian Weinberger. Learning with marginalized corrupted features. In *ICML*, 2013.
- [34] Ishan Misra and Laurens van der Maaten. Self-supervised learning of pretext-invariant representations. In *arXiv preprint arXiv:1912.01991*, 2019.
- [35] Mehdi Noroozi and Paolo Favaro. Unsupervised learning of visual representations by solving jigsaw puzzles. In *ECCV*, 2016.
- [36] Aaron van den Oord, Yazhe Li, and Oriol Vinyals. Representation learning with contrastive predictive coding. In *arXiv preprint arXiv:1807.03748*, 2018.
- [37] Deepak Pathak, Philipp Krahenbuhl, Jeff Donahue, Trevor Darrell, and Alexei A Efros. Context encoders: Feature learning by inpainting. In *CVPR*, 2016.
- [38] Alexander J Ratner, Henry Ehrenberg, Zeshan Hussain, Jared Dunnmon, and Christopher Ré. Learning to compose domain-specific transformations for data augmentation. In *NeurIPS*, 2017.
- [39] Shaoqing Ren, Kaiming He, Ross Girshick, and Jian Sun. Faster r-cnn: Towards real-time object detection with region proposal networks. In *NeurIPS*, 2015.
- [40] Yonglong Tian, Dilip Krishnan, and Phillip Isola. Contrastive multiview coding. In *arXiv preprint arXiv:1906.05849*, 2019.
- [41] Paul Upchurch, Jacob Gardner, Geoff Pleiss, Robert Pless, Noah Snavely, Kavita Bala, and Kilian Weinberger. Deep feature interpolation for image content changes. In *CVPR*, 2017.
- [42] Yulin Wang, Xuran Pan, Shiji Song, Hong Zhang, Gao Huang, and Cheng Wu. Implicit semantic data augmentation for deep networks. In *NeurIPS*, 2019.
- [43] Zhirong Wu, Yuanjun Xiong, Stella Yu, and Dahua Lin. Unsupervised feature learning via non-parametric instance-level discrimination. In *CVPR*, 2018.
- [44] Ting Yao, Yiheng Zhang, Zhaofan Qiu, Yingwei Pan, and Tao Mei. Seco: Exploring sequence supervision for unsupervised representation learning. *arXiv preprint arXiv:2008.00975*, 2020.
- [45] Mang Ye, Xu Zhang, Pong C Yuen, and Shih-Fu Chang. Unsupervised embedding learning via invariant and spreading instance feature. In *CVPR*, 2019.
- [46] Richard Zhang, Phillip Isola, and Alexei A Efros. Colorful image colorization. In *ECCV*, 2016.
- [47] Richard Zhang, Phillip Isola, and Alexei A Efros. Split-brain autoencoders: Unsupervised learning by cross-channel prediction. In *CVPR*, 2017.
- [48] Chengxu Zhuang, Alex Lin Zhai, and Daniel Yamins. Local aggregation for unsupervised learning of visual embeddings. In *ICCV*, 2019.

Appendix

The supplementary material contains: **1)** the theoretical derivation of Eq.(M.8); **2)** the computational complexity analysis of JCL; **3)** the implementation details of pre-training on ImageNet1K (as in Section (M.4.1)); **4)** the experimental settings of the ablation studies (as in Section (M.4.4)); **5)** the details for visualizing similarities and variances distributions (as in Fig.(M.3)).

Note: We use notation Eq.(M.xx) to refer to the equation Eq.(xx) presented in the main paper, and use Eq.(S.xx) to indicate the equation Eq.(xx) in this supplementary material. Similarly, we use Fig./Section/Table (M.xx) and Fig./Section/Table (S.xx) to respectively indicate a certain figure/section/table in the main paper (M.xx) or supplementary material (S.xx).

A Theoretical Derivation of Eq.(M.8)

Firstly, for any random variable \mathbf{x} that follows Gaussian distribution $\mathbf{x} \sim \mathcal{N}(\boldsymbol{\mu}, \boldsymbol{\Sigma})$, where $\boldsymbol{\mu}$ is the expectation of \mathbf{x} , $\boldsymbol{\Sigma}$ is the variance of \mathbf{x} , we have the moment generation function that satisfies:

$$\mathbb{E}_{\mathbf{x}}[e^{\mathbf{a}^T \mathbf{x}}] = e^{\mathbf{a}^T \boldsymbol{\mu} + \frac{1}{2} \mathbf{a}^T \boldsymbol{\Sigma} \mathbf{a}}. \quad (10)$$

Under the Gaussian assumption $\mathbf{k}_i^+ \sim \mathcal{N}(\boldsymbol{\mu}_{k_i^+}, \boldsymbol{\Sigma}_{k_i^+})$, along with Eq.(S.10), we find that Eq.(M.7) immediately reduces to:

$$\text{Eq.(M.7)} = \log \left[\exp(\mathbf{q}_i^T \boldsymbol{\mu}_{k_i^+} / \tau + \frac{1}{2\tau^2} \mathbf{q}_i^T \boldsymbol{\Sigma}_{k_i^+} \mathbf{q}_i) + \sum_{j=1}^K \exp(\mathbf{q}_i^T \mathbf{k}_{i,j}^- / \tau) \right] - \mathbf{q}_i^T \boldsymbol{\mu}_{k_i^+} / \tau. \quad (11)$$

Since the statistics are more/less informative in the later/beginning of the training, we scale the influence of $\boldsymbol{\Sigma}_{k_i^+}$ by multiplying it with a scalar λ . Such tuning of λ hopefully stabilizes the training, leading to a modified version of Eq.(S.11):

$$\tilde{\mathcal{L}}_i = \log \left[\exp(\mathbf{q}_i^T \boldsymbol{\mu}_{k_i^+} / \tau + \frac{\lambda}{2\tau^2} \mathbf{q}_i^T \boldsymbol{\Sigma}_{k_i^+} \mathbf{q}_i) + \sum_{j=1}^K \exp(\mathbf{q}_i^T \mathbf{k}_{i,j}^- / \tau) \right] - \mathbf{q}_i^T \boldsymbol{\mu}_{k_i^+} / \tau. \quad (12)$$

This resembles our derivation of Eq.(M.8) in the main paper.

B Computational complexity

Regarding the GPU memory cost, the vanilla formulation explicitly involves a batchsize that is M times larger than the conventional contrastive learning. In contrast, the batchsize for JCL remains the same as the conventional contrastive learning. Although M' positive keys are required to compute the sufficient statistics for JCL, the batchsize and the incurred multiplications (between query and key) are reduced. Particularly, JCL utilizes multiple keys merely to reflect the statistics, which helps JCL more efficiently exploit these samples. Therefore, JCL is more memory efficient than vanilla when they achieve the same performance, and JCL always offers better performance when the both cost similar memories.

C Implementation Details of Pre-Training on ImageNet1K

For all the experiments, we generate augmentations in the same way as in MoCo v2 [9] for pre-training. First, a 224×224 patch is randomly cropped from the resized images. Then color jittering, random grayscale, Gaussian blur, and random horizontal flip are sequentially applied to each patch. We implement ShuffleBN in [18] by concatenating $N \times M'$ positive keys in the batch dimension and shuffling the data before feeding them into the network. In regard of negative samples presented in Eq.(M.8), we update the queue \mathcal{Q} following the design in [18]. In detail, we enqueue the average values of keys $\{\boldsymbol{\mu}_{k_i^+}\}_{i=1}^N$ during training and dequeue the oldest (256 number of) keys in \mathcal{Q} . The momentum value [18] for updating the key encoder is 0.999 and the queue size is 65,536. For pre-training, we use SGD with 0.9 momentum and 0.0001 weight decay. The pre-trained weights of query encoder are extracted as network initialization for downstream tasks.

D Experimental Settings of Ablation Studies

The ablation experiments are conducted on a subset of ImageNet1K (i.e., ImageNet100) following [40]. Specifically, 100 classes are randomly sampled from the primary ImageNet1K dataset, which are utilized for both pre-training and linear classification. The exact classes include:

n02869837, n01749939, n02488291, n02107142, n13037406, n02091831, n04517823, n04589890, n03062245, n01773797, n01735189, n07831146, n07753275, n03085013, n04485082, n02105505, n01983481, n02788148, n03530642, n04435653, n02086910, n02859443, n13040303, n03594734, n02085620, n02099849, n01558993, n04493381, n02109047, n04111531, n02877765, n04429376, n02009229, n01978455, n02106550, n01820546, n01692333, n07714571, n02974003, n02114855, n03785016, n03764736, n03775546, n02087046, n07836838, n04099969, n04592741, n03891251, n02701002, n03379051, n02259212, n07715103, n03947888, n04026417, n02326432, n03637318, n01980166, n02113799, n02086240, n03903868, n02483362, n04127249, n02089973, n03017168, n02093428, n02804414, n02396427, n04418357, n02172182, n01729322, n02113978, n03787032, n02089867, n02119022, n03777754, n04238763, n02231487, n03032252, n02138441, n02104029, n03837869, n03494278, n04136333, n03794056, n03492542, n02018207, n04067472, n03930630, n03584829, n02123045, n04229816, n02100583, n03642806, n04336792, n03259280, n02116738, n02108089, n03424325, n01855672, n02090622

For ablation studies, we adopt ResNet-18 as the backbone and all models are trained for 100 epochs with a batch size of $N = 128$ at the pre-training stage. The learning rate is set to $lr = 0.1$ and is gradually annealed following a cosine decay schedule [32]. For linear classification, all models are trained for 100 epochs with a learning rate of $lr = 10.0$. The learning rate is decreased by 0.1 at 60^{th} and 80^{th} epochs, and the batch size is $N = 256$. Table 3 shows the detailed settings of hyper-parameters for three ablation experiments of the main paper.

Table 3: Hyper-parameters for ablation studies in Section (M.4.4) of the main paper. “/” indicates non-applicable, since the corresponding hyper-parameter is varied for ablation study.

Ablation Studies	Number of positive keys	Strength of augmentation	Temperature for softmax
	M'	λ	τ
Fig.(M.2(a))	/	4.0	0.2
Fig.(M.2(b))	5	/	0.2
Fig.(M.2(c))	5	4.0	/

E Details for Visualizing Similarities and Variances Distributions

For the experiments that visualize the distributions of similarities and variances in Section (M.4.5), we respectively extract features from pre-trained ResNet-18 models of JCL and MoCo v2. At the pre-training stage, the hyper-parameters are set as $\tau = 0.2$, $M' = 9$ and $\lambda = 4.0$ for JCL. For MoCo v2, we use the released code from <https://github.com/facebookresearch/moco> to train a ResNet-18 model. Both JCL and MoCo v2 are trained on the ImageNet100 dataset for 100 epochs. Other hyper-parameters are exactly the same as the settings used in ablation studies. In total, we sample 32,768 images for depicting the histograms in Fig.(M.3). For each image, we randomly generate 32 augmented images and feed these images into the pre-trained network to extract features. The feature vectors are ℓ_2 normalized before computing similarities and variances. For the similarity visualization in Fig.(M.3(a)), cosine similarities of all pairs (32×32 in total) are averaged into a single sample point used for drawing the histogram (hence 32,768 points in Fig.(M.3(a))). Similarly, for visualizing feature variances Fig.(M.3(b)), we use the ℓ_2 normalized features to compute the covariance matrix of augmented images belonging to the same source image, and we average the diagonal values of covariance matrix for each source image into a single sample point to draw the histogram (hence 32,768 points in Fig.(M.3(b))). Note that only using diagonal values of the covariance matrix respects our primary purpose of computing the *dimension – dimension* feature correlations between feature vectors.